Supporting Information

Luminescent cationic MOF and its polymer composite membrane elicit selective sensing of antibiotics and pesticides in water

Subhajit Dutta,[†a] Writakshi Mandal,[†a] Aamod V. Desai,[a] Sahel Fajal,[a] Gourab K. Dam,[a] Soumya Mukherjee,*[b] Sujit K. Ghosh* [a,c]

[a]Department of Chemistry, Indian Institute of Science Education and Research (IISER), Dr. Homi Bhabha Road, Pashan, Pune411008, India. *E-mail: sghosh@iiserpune.ac.in*

[b]Bernal Institute, Department of Chemical Sciences, University of Limerick, Limerick V94 T9PX, Ireland. *E-mail: Soumya.Mukherjee@ul.ie*

[c]Centre for Water Research (CWR), Indian Institute of Science Education and Research (IISER), Pune 411008, India.

[†] These authors contributed equally to this work.

Experimental Section:

Physical measurements:

Powder X-ray diffraction (PXRD) patterns were recorded by a Bruker D8 Advanced X-ray diffractometer in a 2θ range of 5° to 40° by using Cu Kα radiation (λ = 1.5406 Å) with a scan speed of 0.9° min^{-1}. Fourier transform infrared spectra (FT-IR) spectra were collected using a NICOLET 6700 IR spectrometer. Fluorescence spectroscopic studies were performed with a Jobin Yvon Fluoromax-4 spectrofluorometer. Steady-state photoluminescence studies were recorded on a Fluorolog-3 spectrofluorometer (HORIBA Scientific). Thermogravimetric analysis (TGA) was conducted using a Perkin Elmer STA6000 TG analyser under N_2 atmosphere, keeping the heating rate constant at 10 °C min^{-1}. Field emission scanning electron microscopy (FESEM) studies and energy dispersive X-ray (EDX) data were acquired from a FEI Quanta 3D dual beam ESEM. Confocal laser scanning microscope (Zeiss, Oberkochen, Germany Model LSM 10) was used to achieve background-free high-resolution microscopy images. The PLQYs data provided in the manuscript is absolute value that determined with an integrating sphere. The absolute photoluminescence quantum yields (PLQY) were measured with a Horiba Fluoromax 4 spectrophotometer equipped with a SC-30 integrating sphere.

X-ray structural studies:

Single crystal X-ray data of **iMOF-14C** was acquired at 150 K from Bruker D8 Venture Duo X-ray diffractometer equipped with a Microfocus X-ray source (operated at 50 W; 50 kV/1 mA) and graded multilayer optics for monochromatic Mo Kα radiation (λ = 0.71073 Å) with a focused X-ray beam and a Photon 100 CMOS chip-based detector system. The crystal was mounted on nylon Cryo Loops (Hampton Research) with Paraton-N (Hampton Research). The data integration and reduction were processed with SAINT software.[1] A multi-scan absorption correction was applied to the collected reflections.[2] The structure was solved by a direct method using SHELXTL[3,4] and was refined on F^2 with a full-matrix least-squares technique using the SHELXL-2014/7 [5] program package within the WINGX [6] programme. All the H atoms were refined anisotropically. H atoms were located in successive difference Fourier maps, and they were treated as riding atoms using SHELXL default parameters. The structures were examined using the *Adsym* subroutine in PLATON to assure that no additional symmetries could be applied to the models. The SQUEEZE option[7] was used to eliminate the contribution from the disordered guest molecules. CCDC number 2225079 for **iMOF-14C** contains the supplementary crystallographic data for this paper.

Analyte preparation:

First, 1M aqueous stock solutions of all antibiotics and pesticides were prepared.

Titration with NFT, NFZ, CHPS, Nitrofen and other competing analytes with iMOF-14C:

1 mg of crystalline powdered **iMOF-14C** was taken in a quartz cuvette and 2 mL water was added to that. Initial luminescence spectra of **iMOF-14C** in water was recorded by exciting it at 330 nm (PL spectra recorded in the range of 350-650 nm). To the dispersed MOF powder in water, we added stock solutions of each antibiotic and pesticide (20 μL to 300 μL) and the spectra were recorded for each addition. With each addition of nitrofuran (NFT, NFZ) antibiotics and nitrofen and chloropyriphos pesticides, gradual quenching in the fluorescence emission could be observed, but in case of the other antibiotics and pesticides, there are only minimal quenching to the PL spectra. As competing studies, we conducted binary selectivity assays with a range of other antibiotics (STZ, TTC, SGD, SP, KCS, CPL, AC, SMC) with NFZ and NFT individually, these are not nitro-functionalised, in essence. Similar competing experiments were performed with pesticides also. In a typical experiment, 1 mg **iMOF-14C** was taken in 2 mL of water, and 300 μL of a non-quenching antibiotic was added, one at a time. To this solution, 300 μL of NFZ was spiked, and the corresponding spectra were recorded. This allowed us to evaluate the response of our probe(s) towards other competing analytes (included in the bar diagram profiles, Figures 3c, 3f, S25, S26). We have recorded the distinct PL responses of the MOF in the presence of competing antibiotics and pesticides. By combining the dual responses, we determined the selectivity of **iMOF-14C** towards antibiotics (NFZ, NFT) and pesticides (nitrofen, chloropyriphos), each in presence of other competing antibiotics and pesticides.

Detection limit calculation:

To determine detection limits, respective antibiotics and pesticides (20 – 200 μL, 1 mM stock solutions) were added to the probe (desolvated **iMOF-14C**) (1 mg, in 2 mL water) and fluorescent intensity was recorded. By plotting fluorescence intensity with increasing concentration of the oxo-anions, slope (m) of graph were calculated from there. Further, the standard deviation (σ) was calculated from five blank measurements. Detection limit is calculated according to the formula:[8]

$$\text{Detection limit: } (3\sigma / m)$$

Synthesis procedure of iMOF-14C based mixed matrix membranes (MMMs):

In this work, we have prepared a mixed matrix membrane based on a composite mixture of **iMOF-14C** with a polymer, polyvinylidine fluoride (PVDF), following up on a reported protocol.[8] 150 mg of PVDF was taken in 2 mL of DMF, and stirred at room temperature for 24 h, resulting in a viscous, sticky solution.

50 mg of powder **iMOF-14C** was then added to the PVDF-DMF mixture, and stirred for another 24 hours to achieve homogeneity. This mixture was cast onto aluminium foil using a regular scraper to prepare a flat, thin sheet membrane. The cast membrane was dried and soaked in DI water to ensure its fast delamination. The obtained free-standing film was dried at the end.

Supporting information figures:

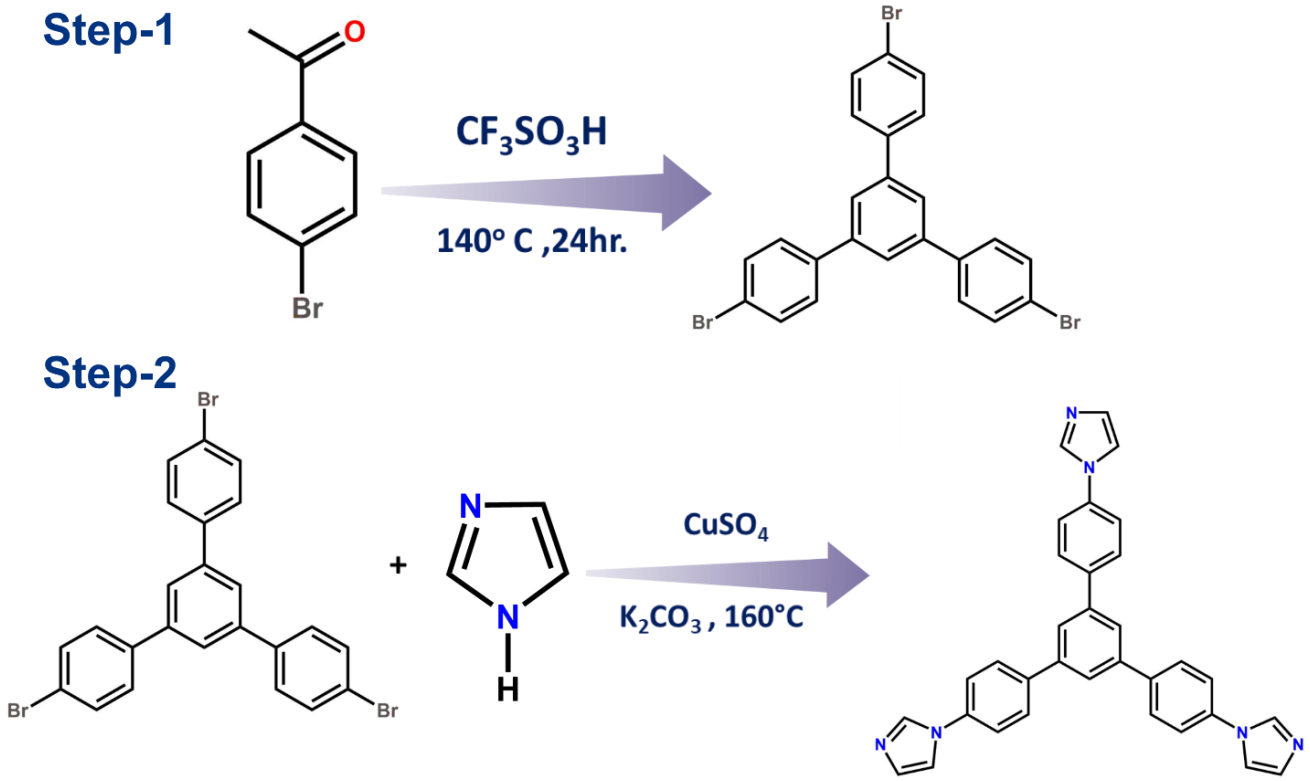

Scheme S1: Synthesis scheme affording the ligand (L).

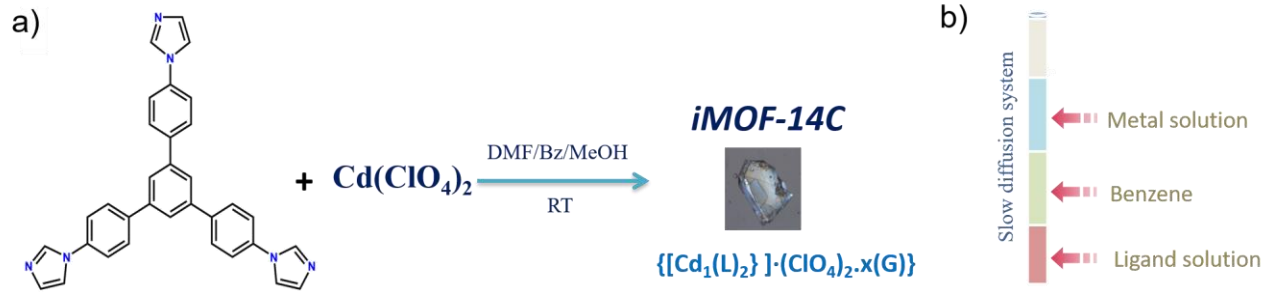

Scheme S2: a) Synthesis scheme affording the MOF, **iMOF-14C**; b) schematic illustration of the slow-diffusion setup.

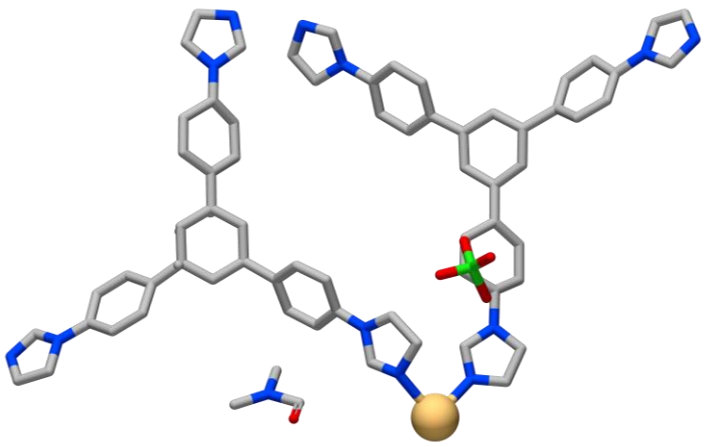

Figure S1: Asymmetric unit of **iMOF-14C** (H atoms omitted for clarity, (colour codes: Grey - C, Blue - N, Yellow – Cd, Red – O, Green - Cl).

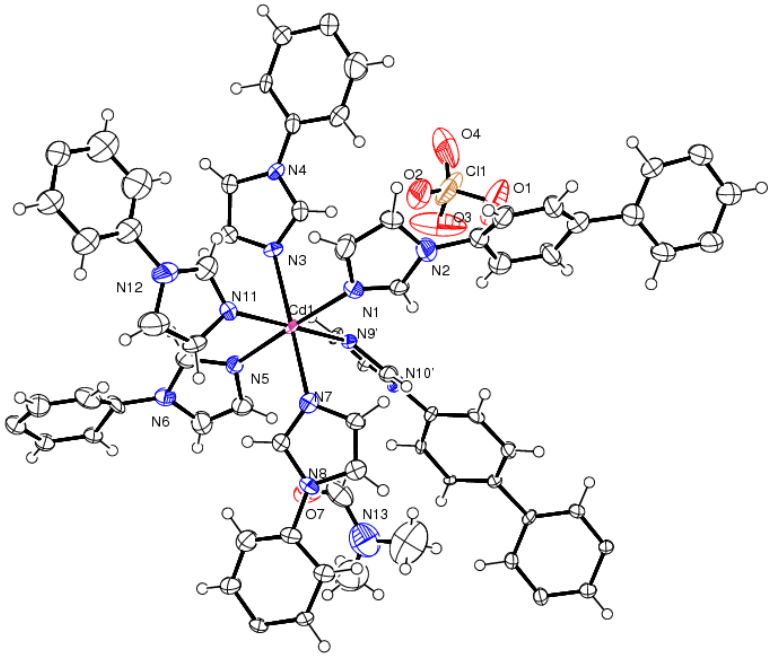

Figure S2: ORTEP diagram of the asymmetric unit in **iMOF-14C**, represented using thermal ellipsoids (each atom at 50% probability).

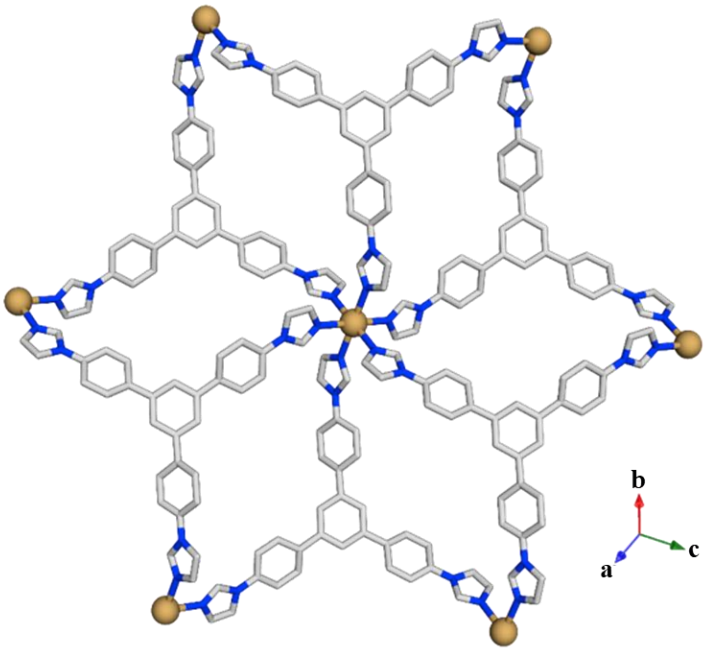

Figure S3: Coordination environment of **iMOF-14C** (H atoms are omitted for clarity, (colour codes: Grey - C, Blue - N, Yellow – Cd, Red – O, Green – Cl), ClO_4^- omitted because of clarity.

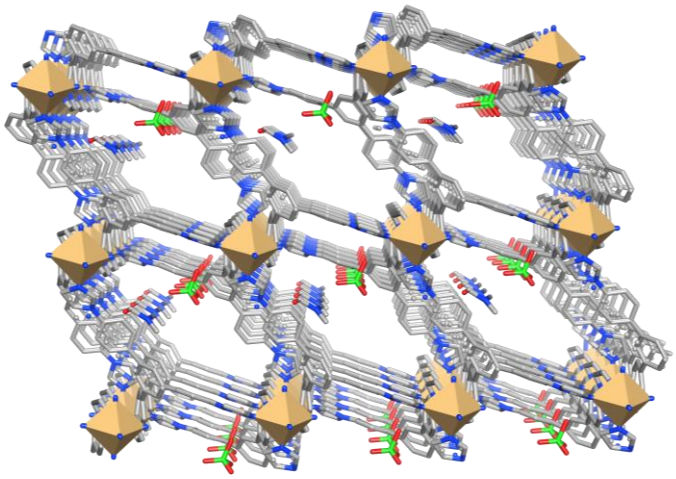

Figure S4: Perspective view of packing in **iMOF-14C** along *c* axis with ClO_4^- anions and DMF molecules inside the pore. H atoms omitted for clarity (colour codes: Grey - C, Blue - N, Yellow – Cd, Red – O, Green – Cl).

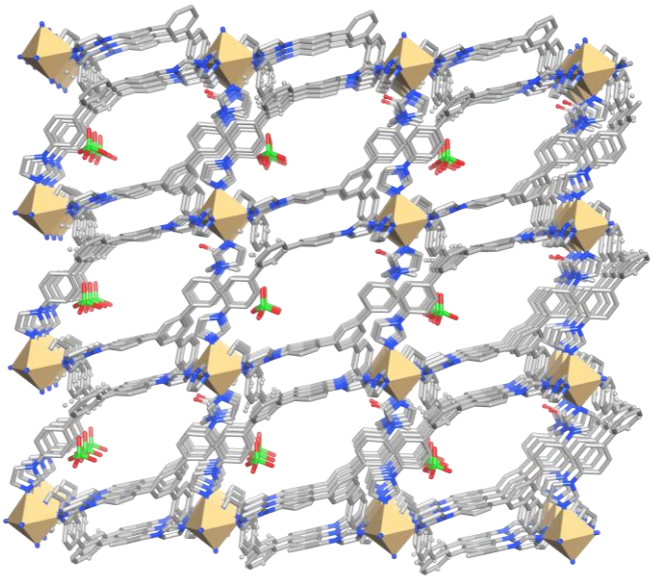

Figure S5: Perspective view of packing in **iMOF-14C** along *a* axis with ClO_4^- anions and DMF molecules inside the pore. H atoms omitted for clarity (colour codes: Grey - C, Blue - N, Yellow – Cd, Red – O, Green – Cl).

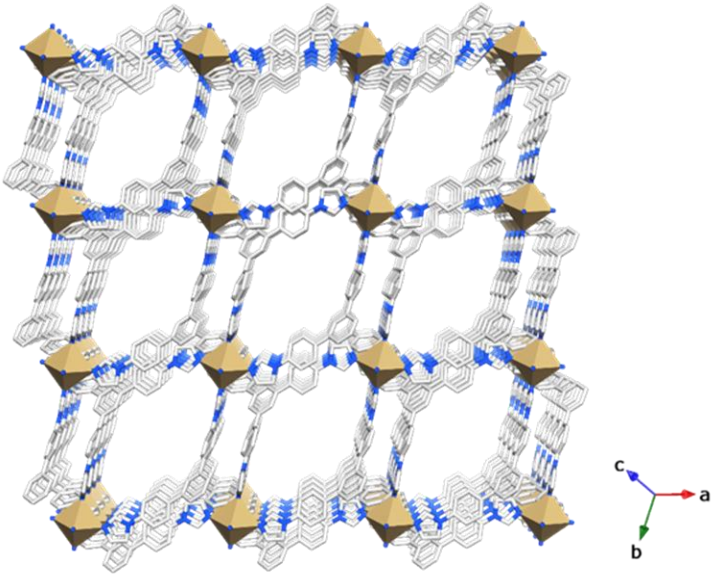

Figure S6: Orthographic view of the packing in **iMOF-14C** (colour codes: Grey - C, Blue - N, Yellow – Cd, Red – O, Green - Cl), ClO_4^- anions and H atoms omitted for clarity.

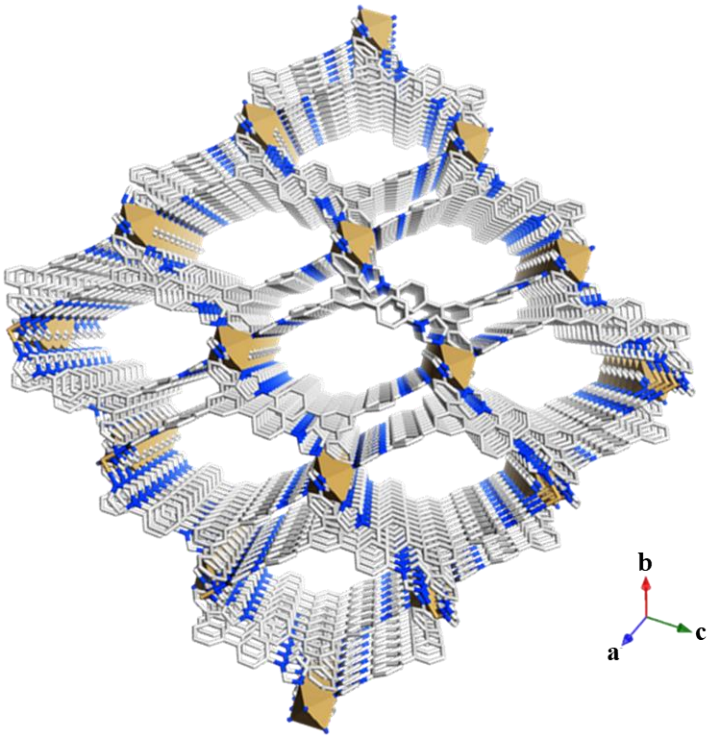

Figure S7: Perspective view of packing in **iMOF-14C** (colour codes: Grey - C, Blue - N, Yellow – Cd, Red – O, Green - Cl), ClO_4^- anions and H atoms omitted for clarity.

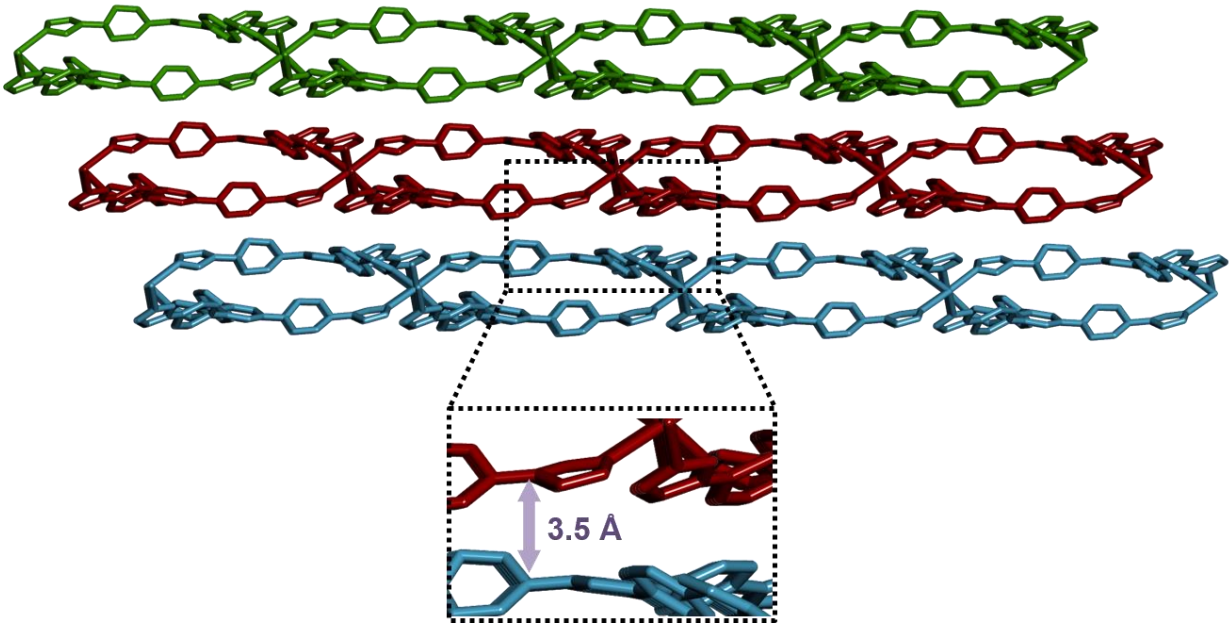

Figure S8: Packing diagram of **iMOF-14C**, showing the distance between two successive 2D layers.

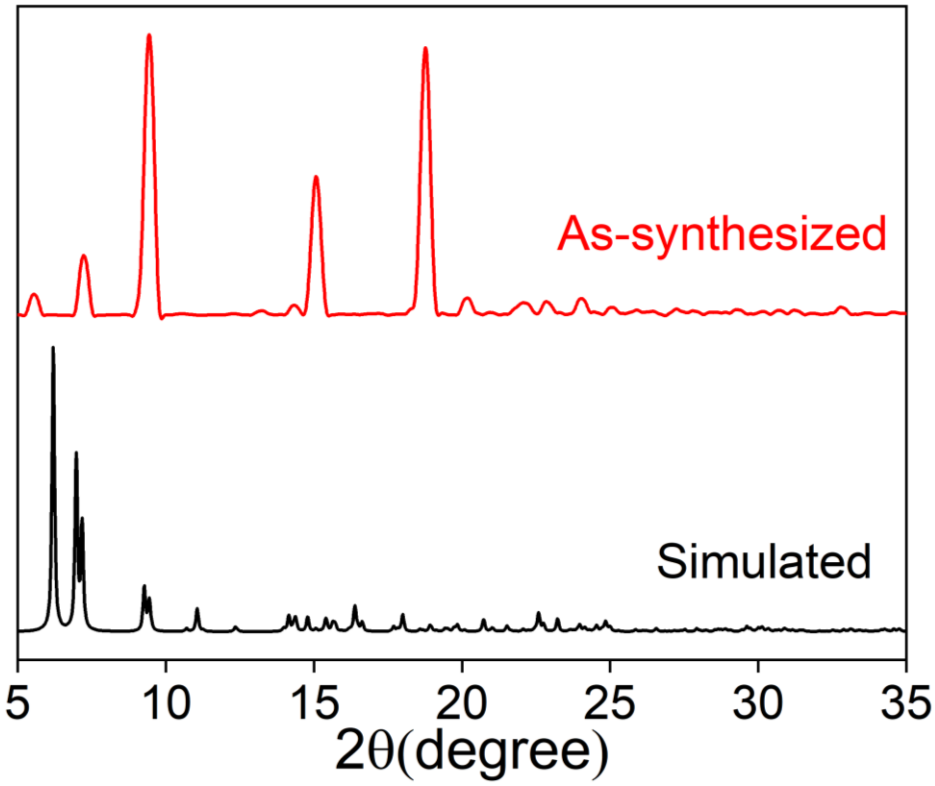

Figure S9: Powder X-ray diffraction patterns of **iMOF-14C**.

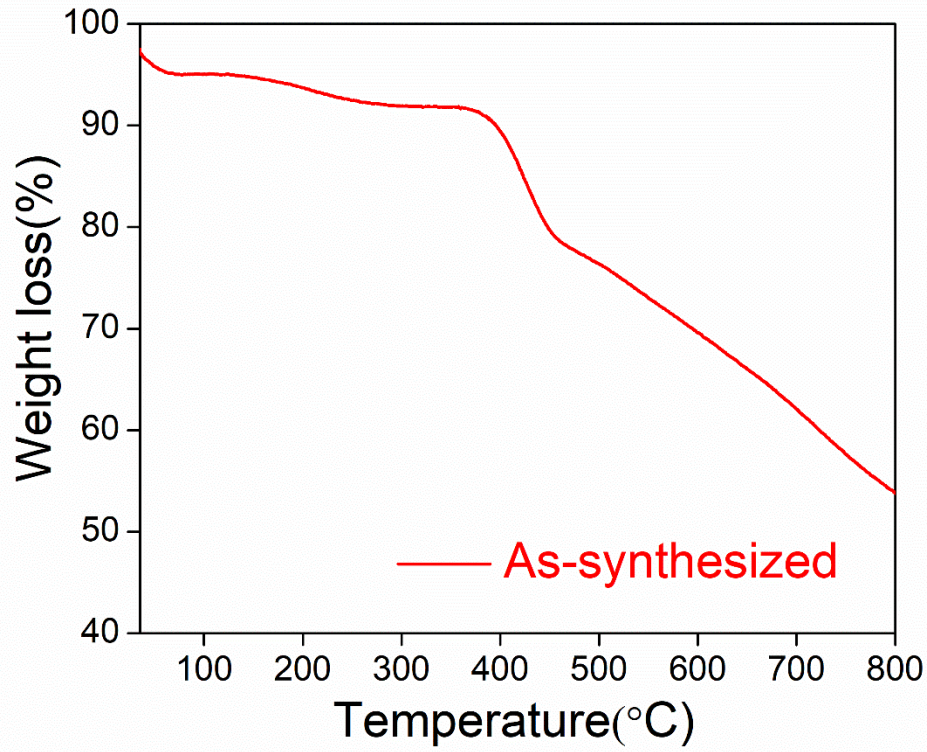

Figure S10: TGA trace recorded for the as-synthesised phase of **iMOF-14C**.

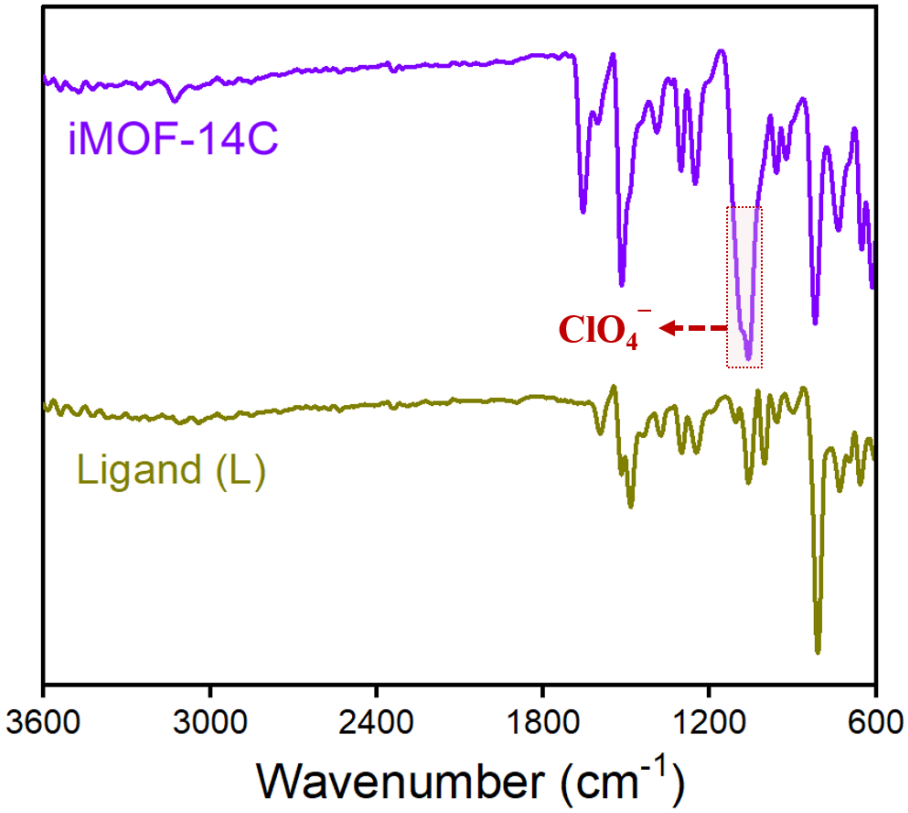

Figure S11: IR spectra of **iMOF-14C** including characteristic peaks of the framework along with that of the ClO_4^- anions.

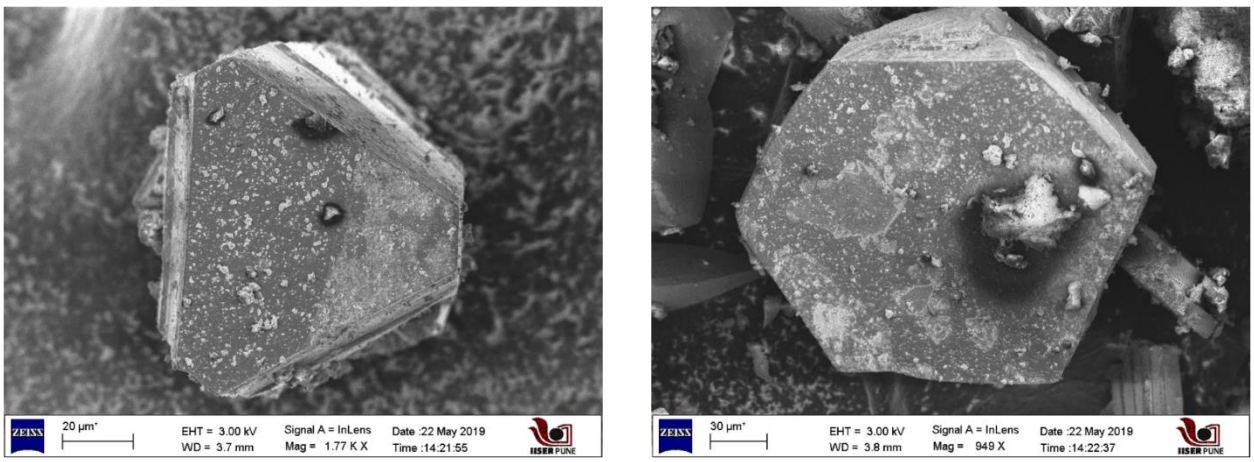

Figure S12: FESEM images of **iMOF-14C**.

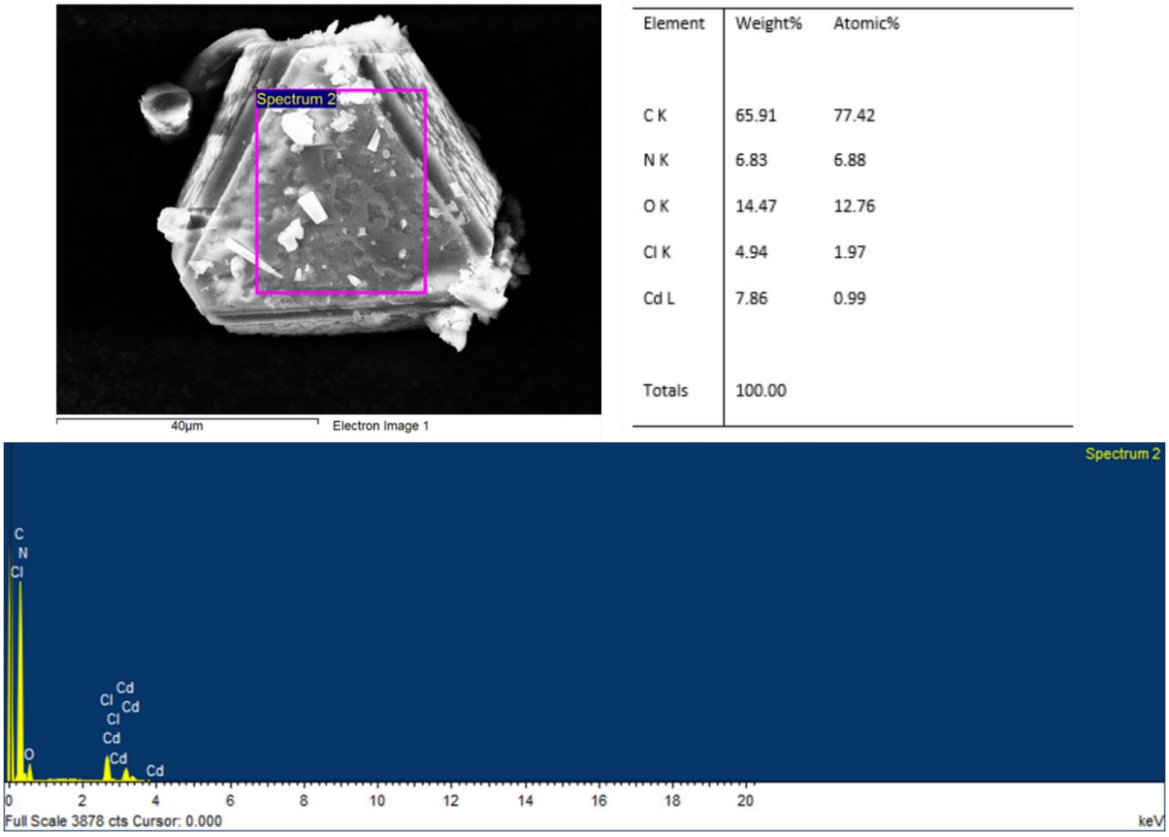

Figure S13: EDX analysis of **iMOF-14C**.

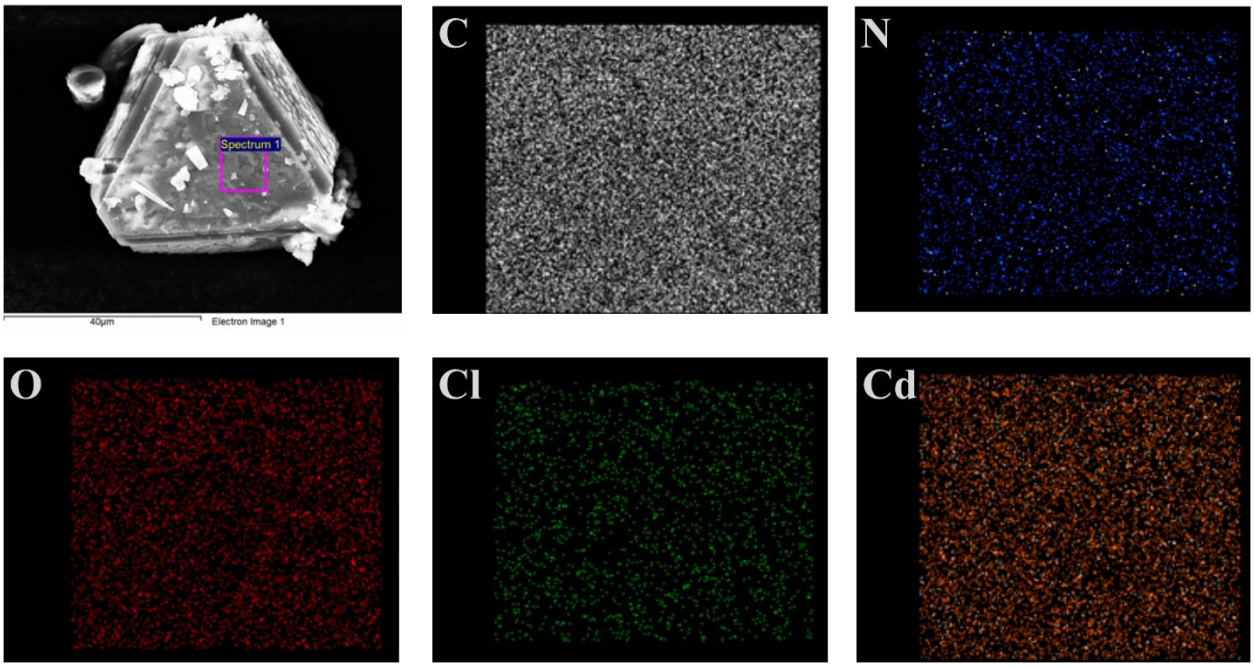

Figure S14: Elemental mapping images for **iMOF-14C**.

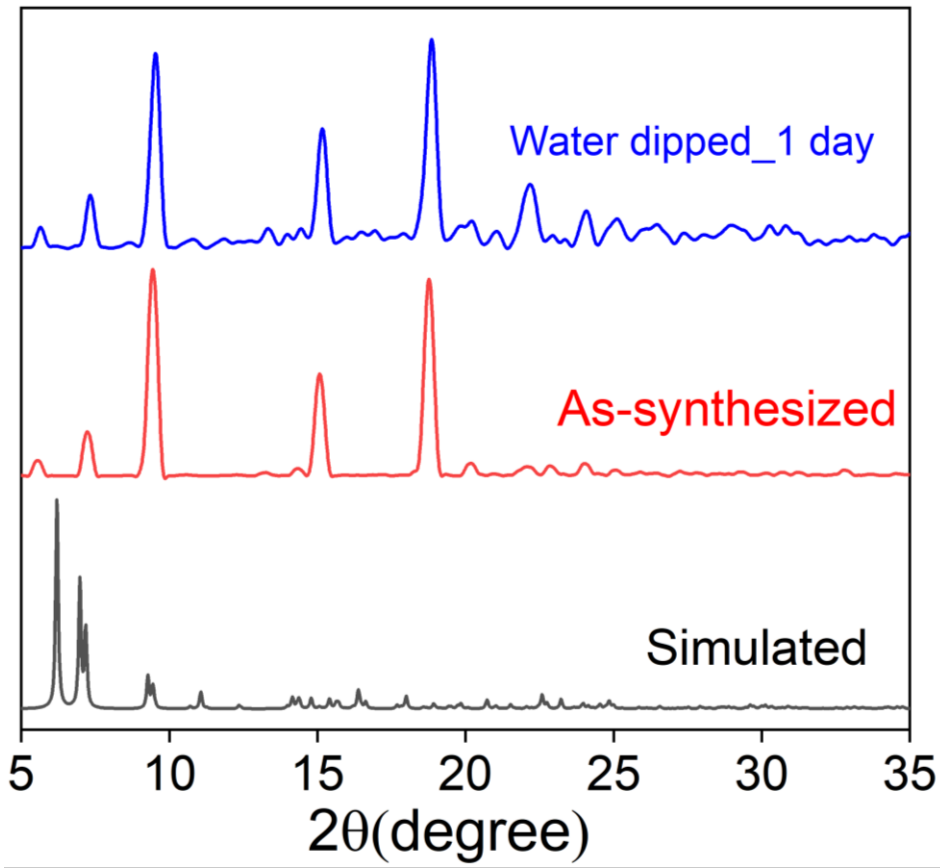

Figure S15: Powder X-ray diffraction patterns of **iMOF-14C**, exhibiting its hydrolytic stability.

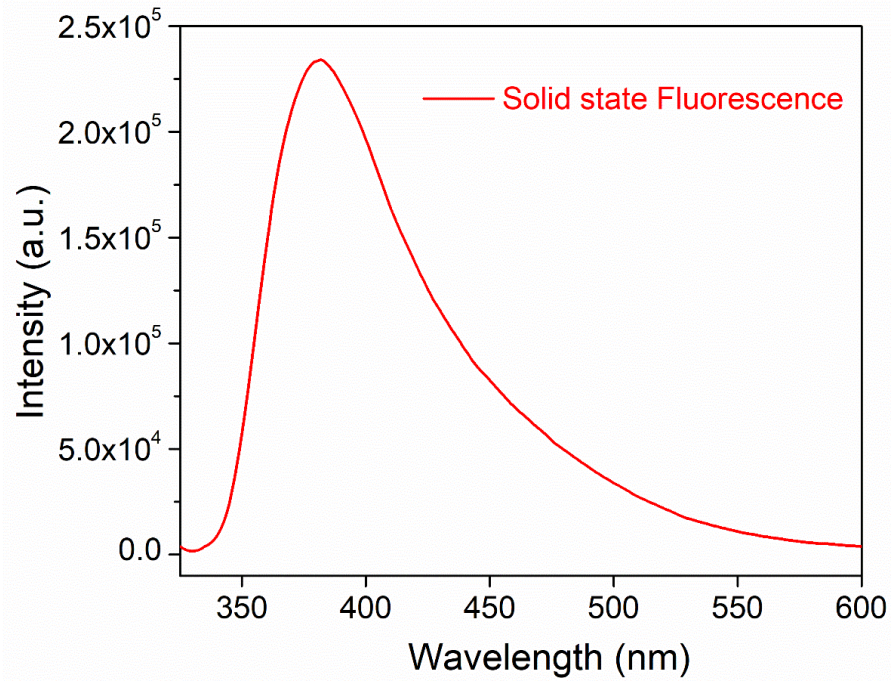

Figure S16: Solid state fluorescence spectra of **iMOF-14C** (λ_{ex}= 330nm).

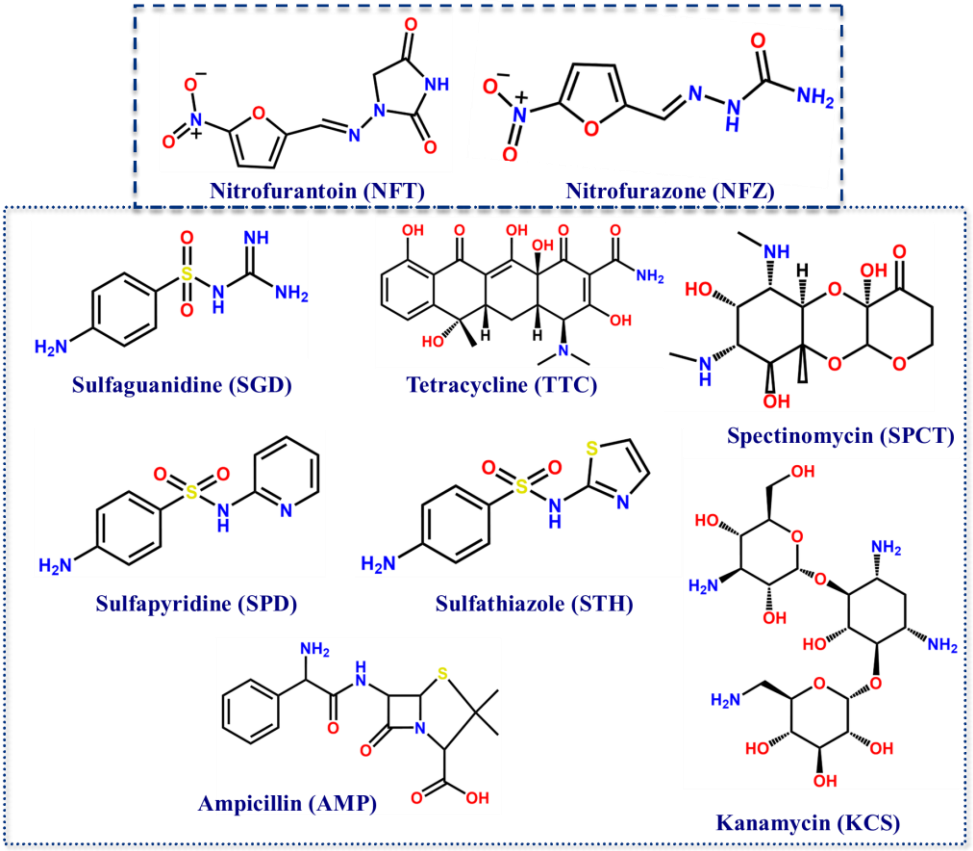

Figure S17: Chemical structures of several antibiotics used in this study.

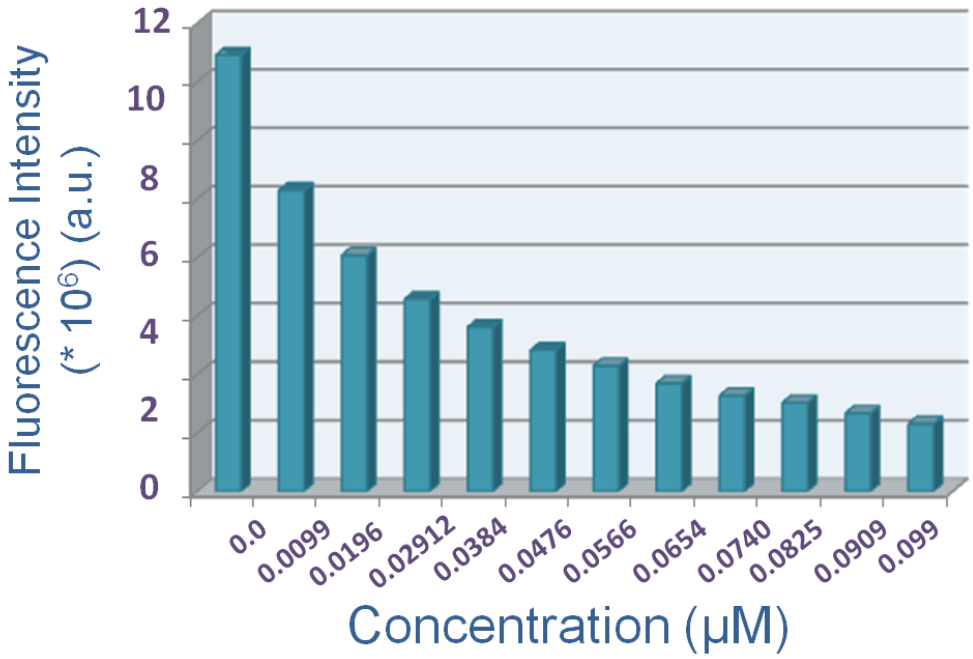

Figure S18: Changes to the fluorescence intensity of **iMOF-14C** in water, with increasing concentration of the **NFT** anions at 378 nm.

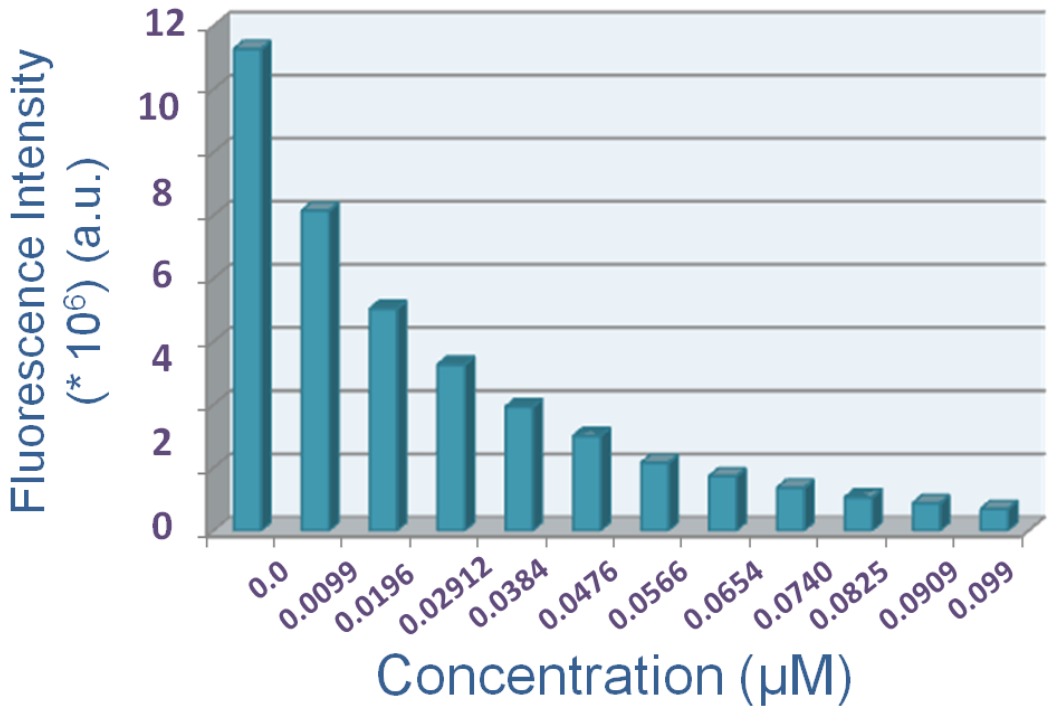

Figure S19: Changes to the fluorescence intensity of **iMOF-14C** in water, with increasing concentration of the **NFZ** anions at 378 nm.

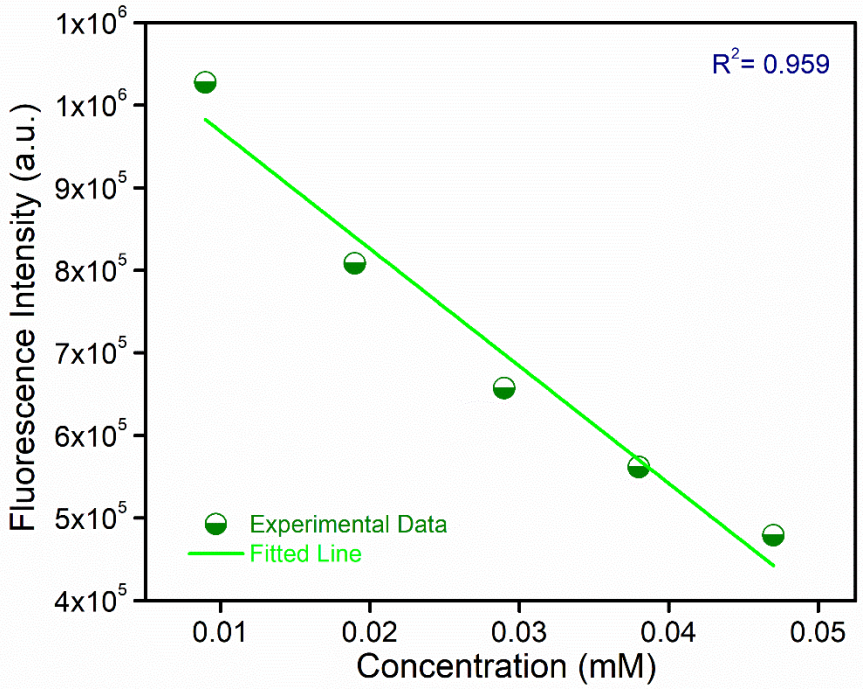

Figure S20: Linear region of fluorescence intensity of probe upon addition of NFT λ_{em}= 378 nm (upon excitation at 330 nm).

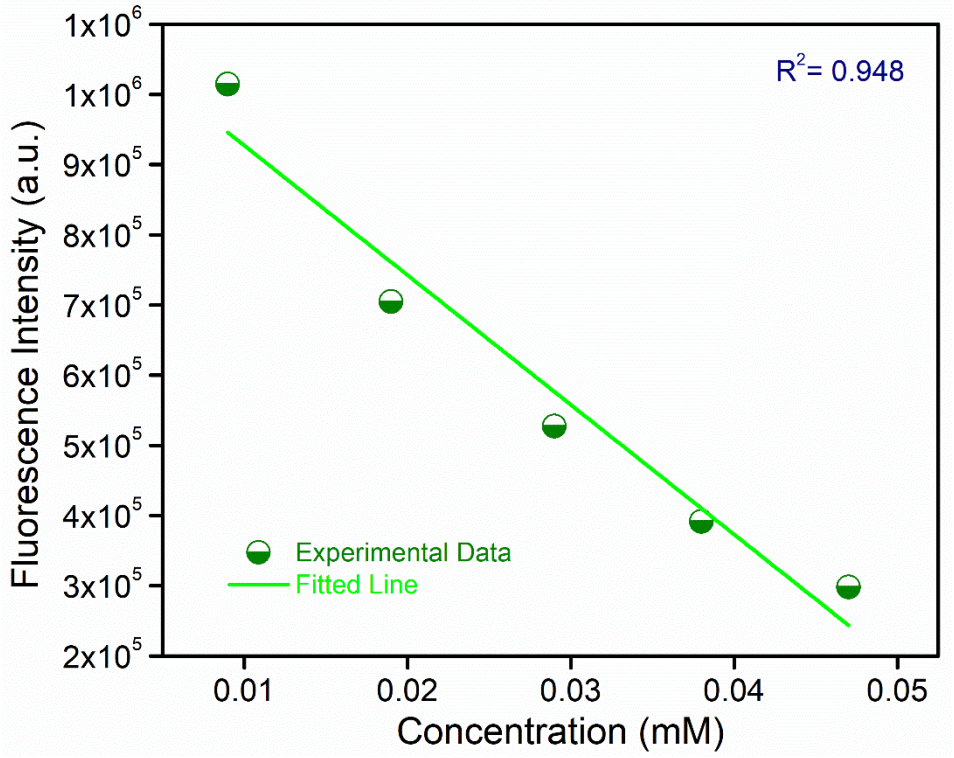

Figure S21: Linear region of fluorescence intensity of probe upon addition of NFZ; λ_{em}= 378 nm (upon excitation at 330 nm).

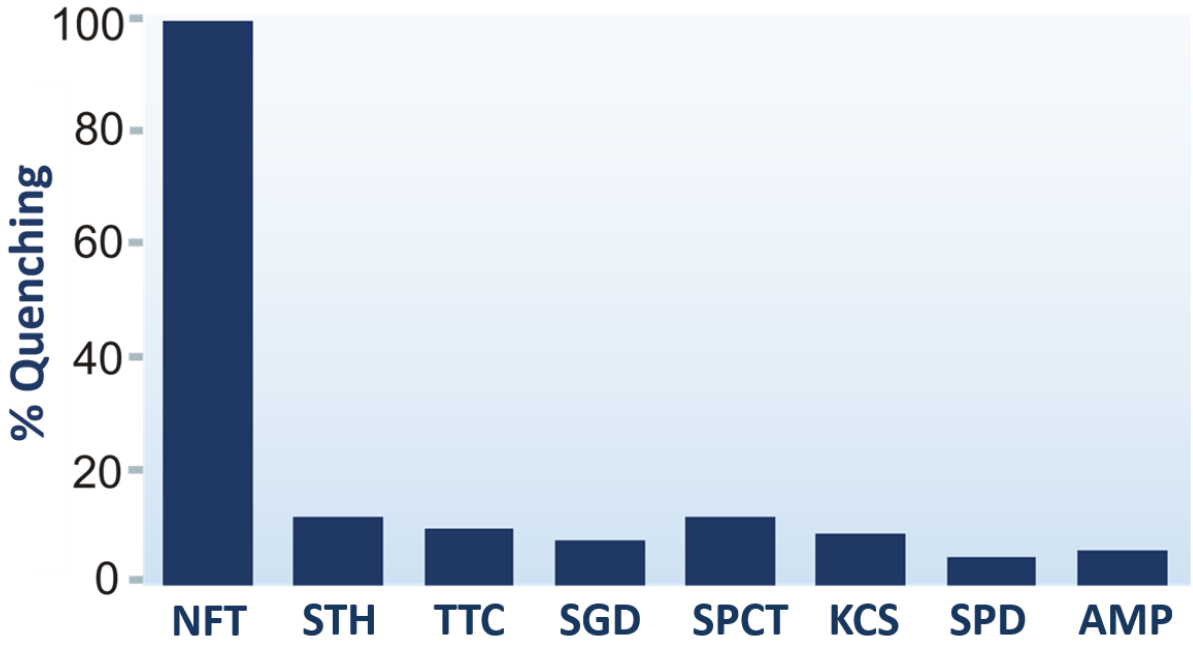

Figure S22: Percentage quenching of fluorescence emission of **iMOF-14C** towards NFT, and other competing antibiotics.

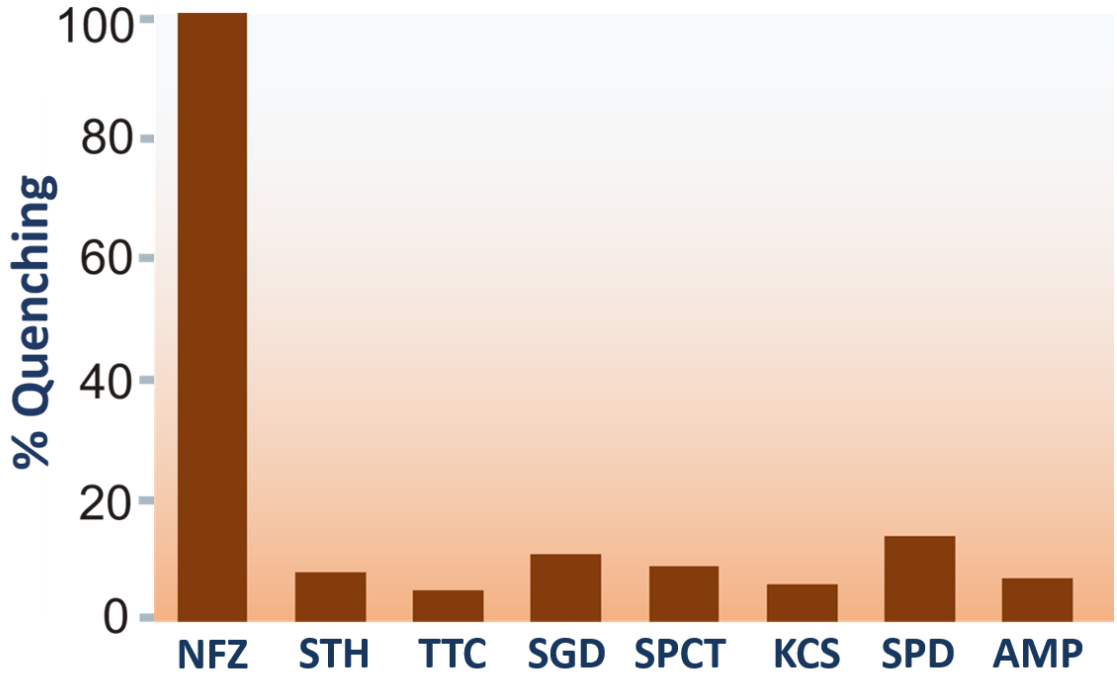

Figure S23: Percentage quenching of fluorescence emission of **iMOF-14C** towards NFZ, and other competing antibiotics.

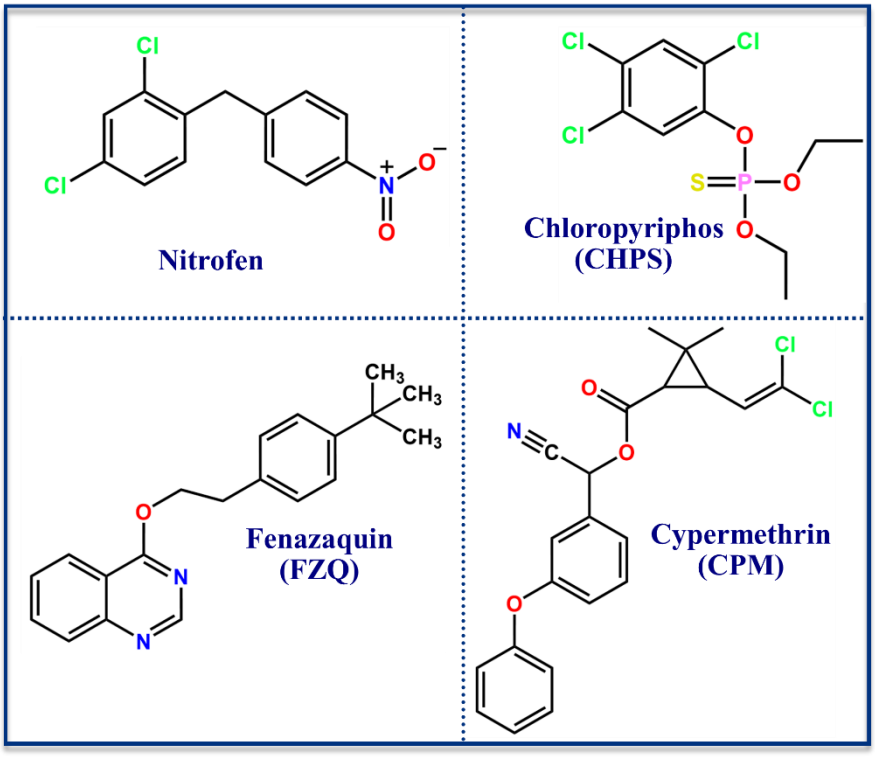

Figure S24: Chemical structures of various pesticides used in this sensing study.

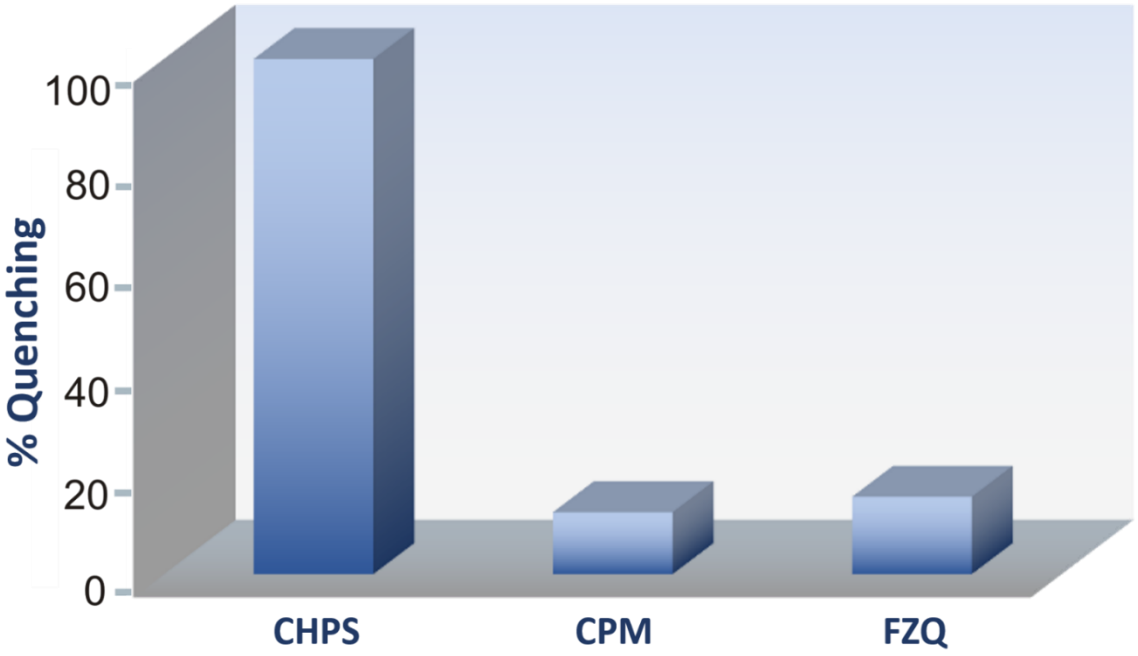

Figure S25: Percentage quenching of fluorescence emission of **iMOF-14C** towards CHPS, and other pesticides.

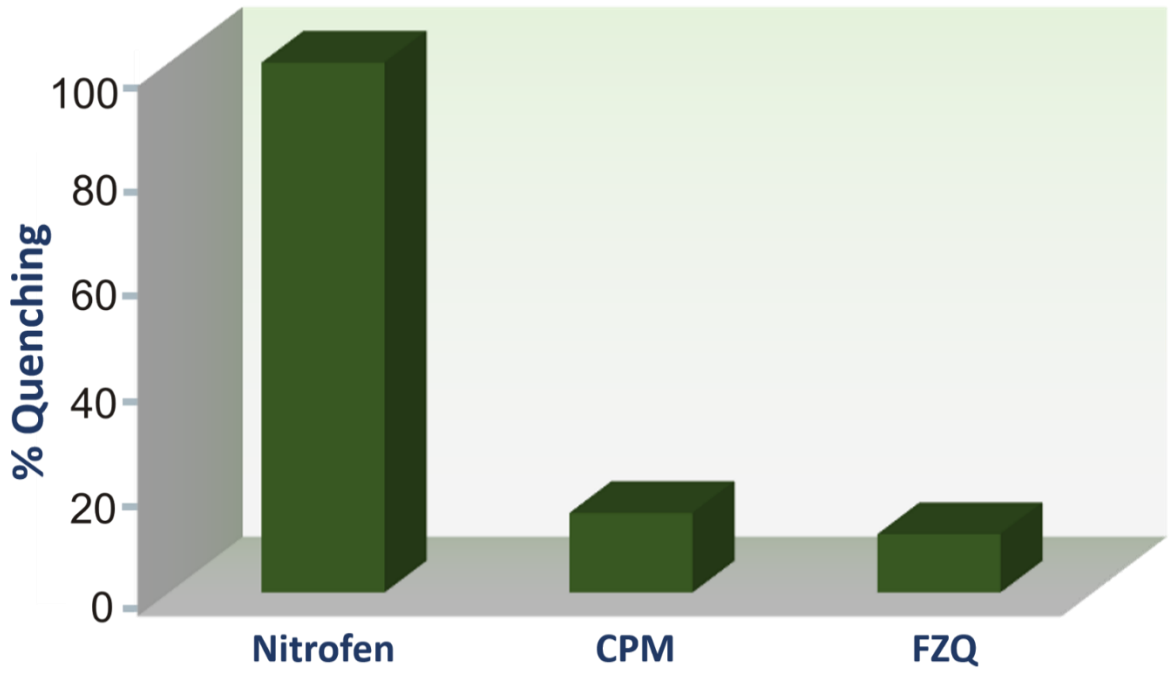

Figure S26: Percentage quenching of fluorescence emission of **iMOF-14C** towards nitrofen, and other pesticides.

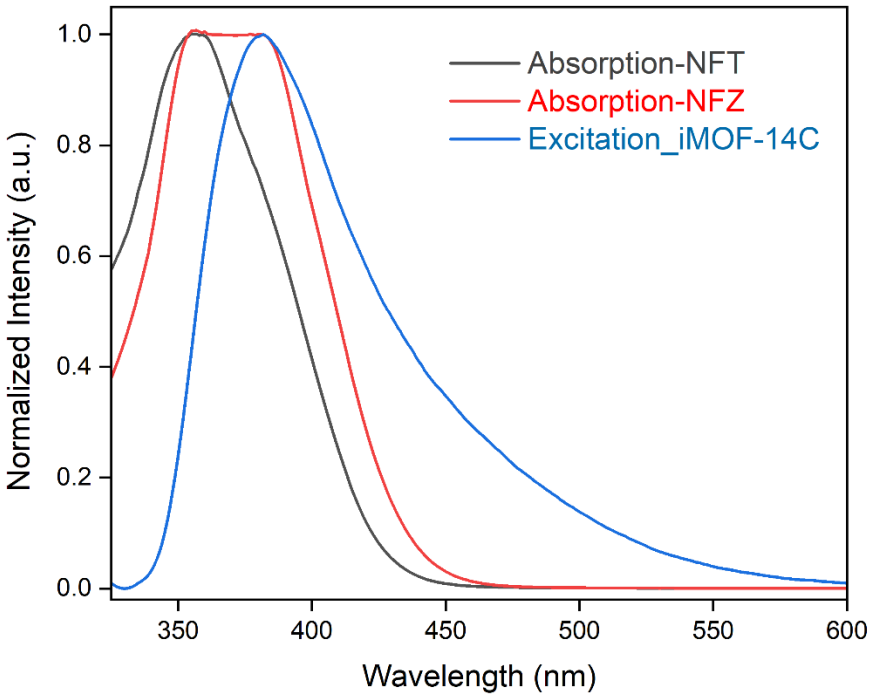

Figure S27: Spectral overlap between the UV−vis spectra of different antibiotics and the fluorescence emission spectra of **iMOF-14C**.

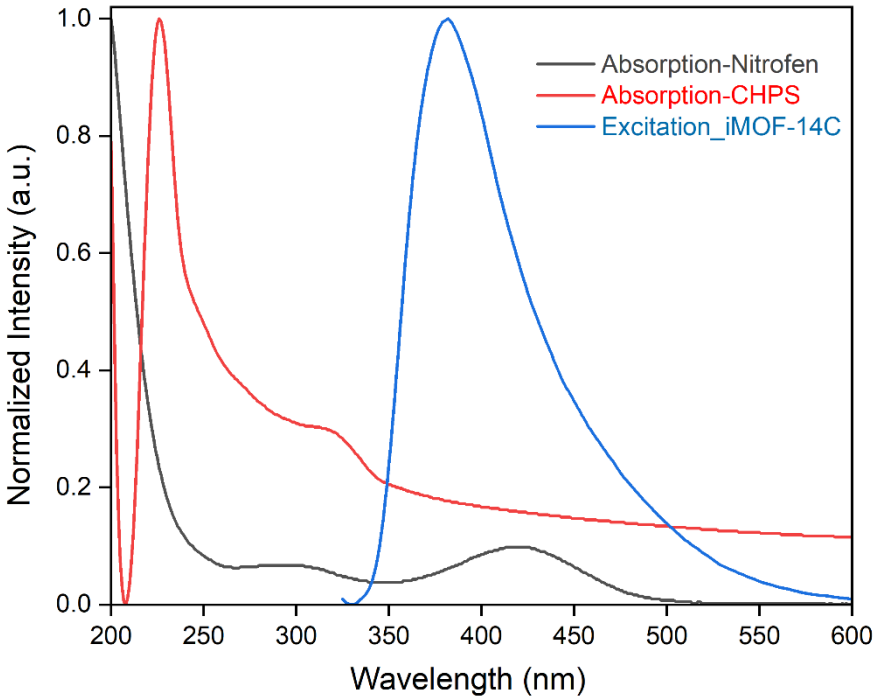

Figure S28: Spectral overlap between the UV−vis spectra of different pesticides and the fluorescence emission spectra of **iMOF-14C**.

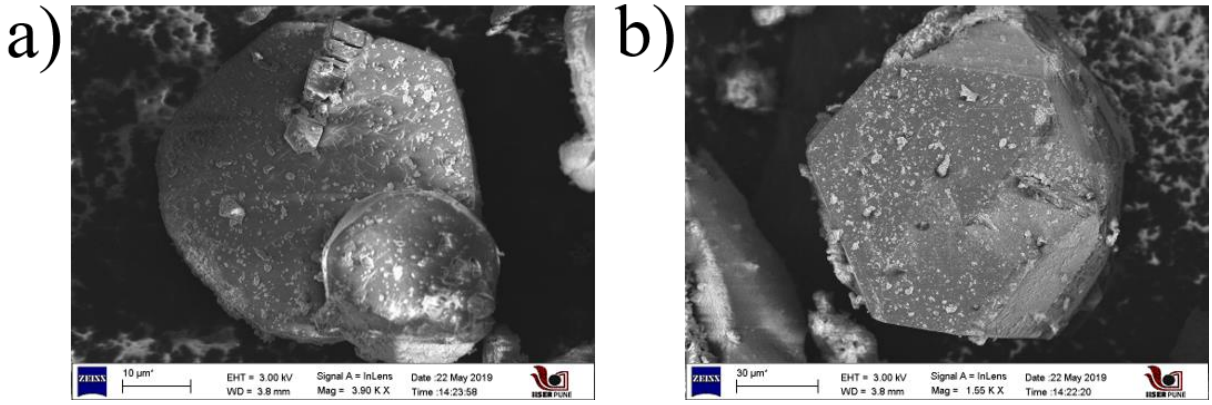

Figure S29: FESEM images of the post-sensing phase of **iMOF-14C**.

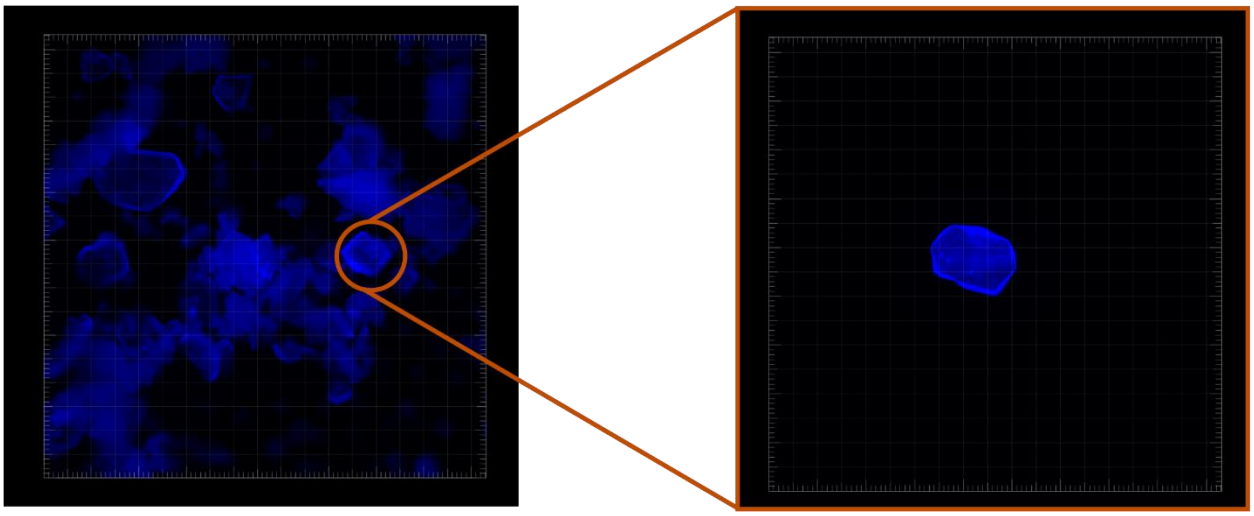

Figure S30: Confocal fluorescence images of **iMOF-14C** upon excitation at 330 nm.

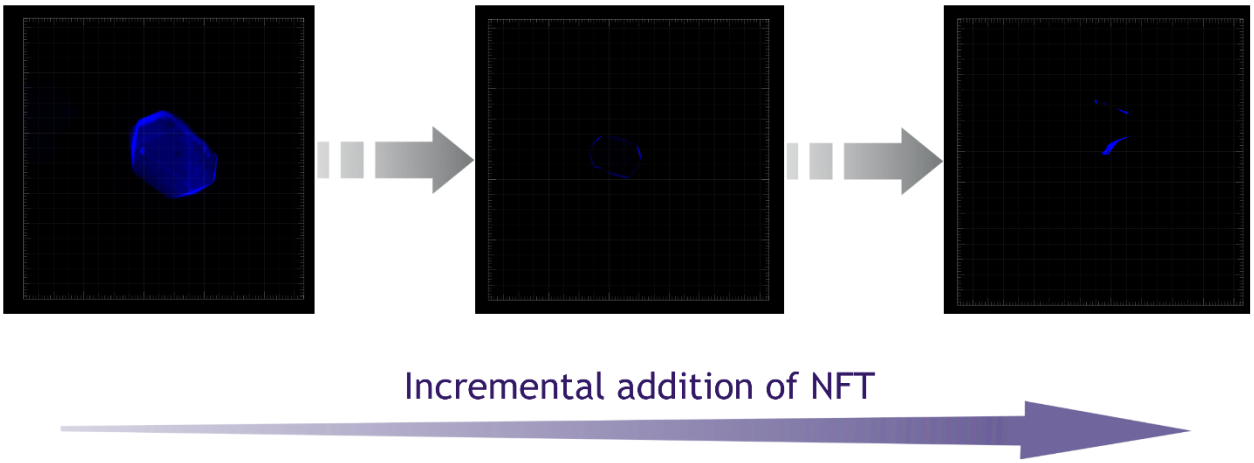

Figure S31: Changes monitored by confocal fluorescence imaging of **iMOF-14C**, upon incremental addition of NFT.

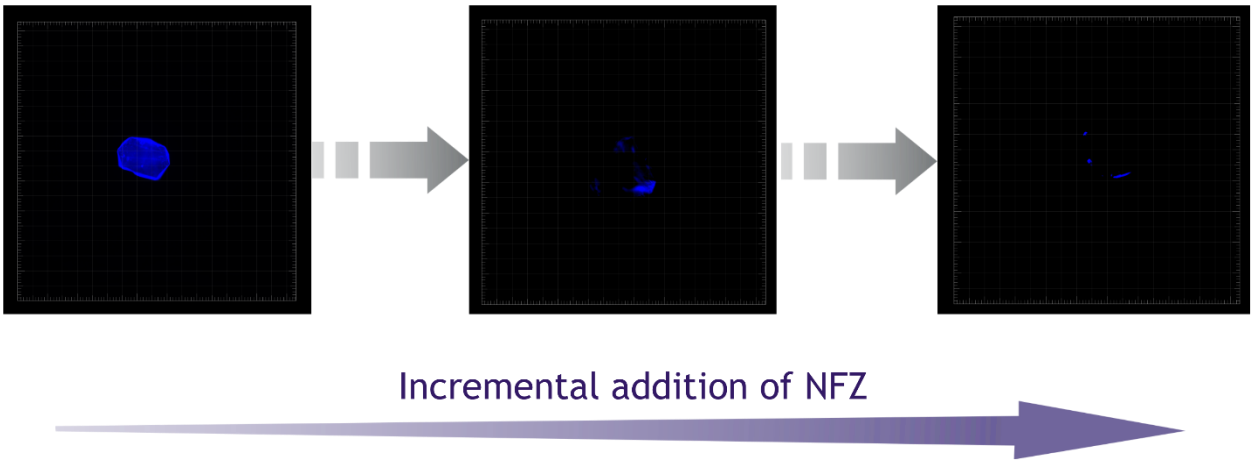

Figure S32: Changes monitored by confocal fluorescence imaging of **iMOF-14C**, upon incremental addition of NFZ.

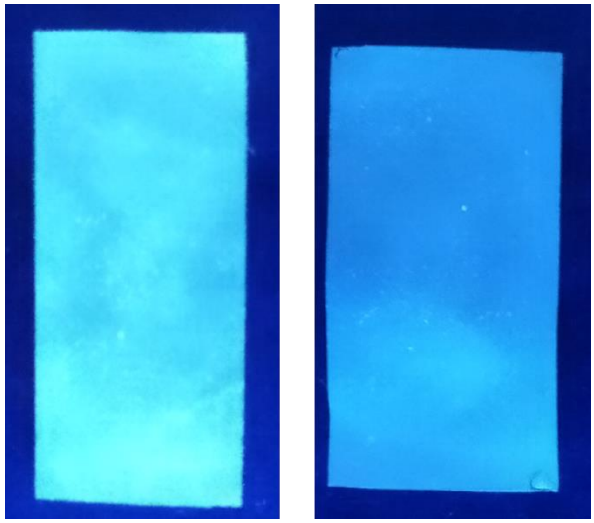

Figure S33: Images of self-standing **iMOF-14C@PVDF** MMMs under UV light.

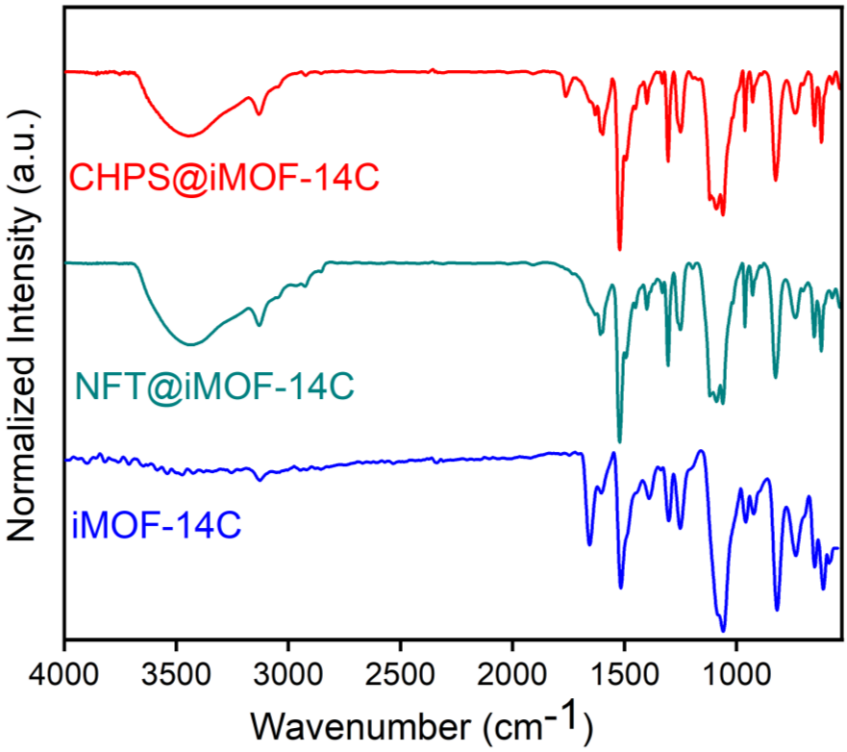

Figure S34: IR spectra of **iMOF-14C** upon treating with NFT and CHPS.

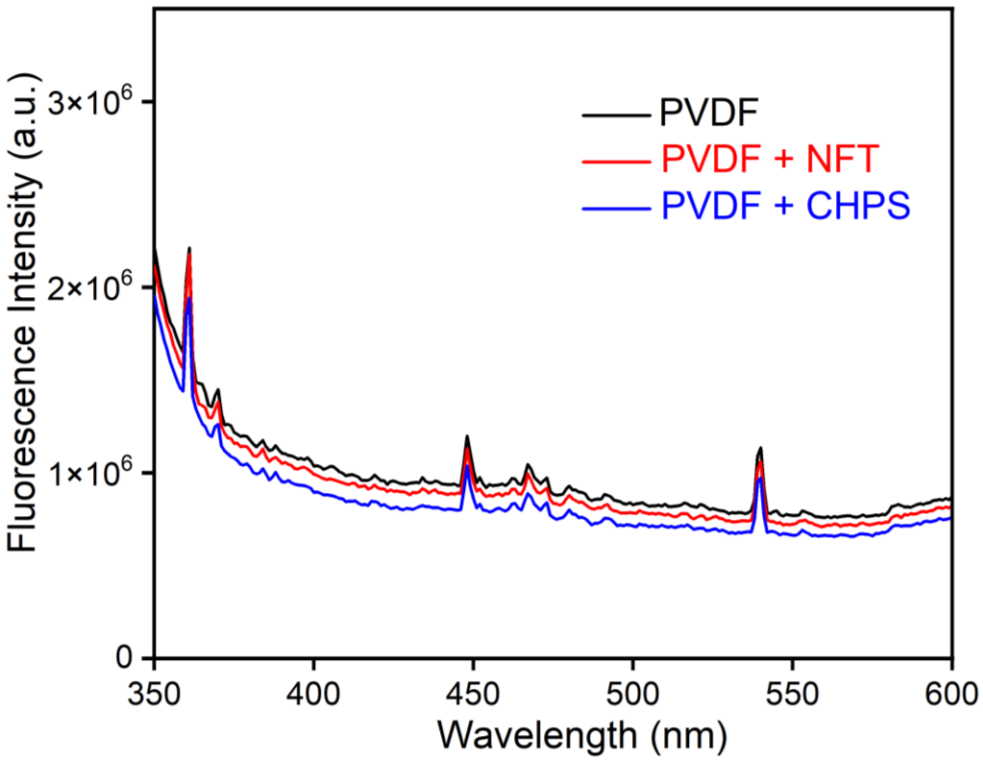

Figure S35: Fluorescence emission spectra of PVDF, PVDF@NFT and PVDF@CHPS.

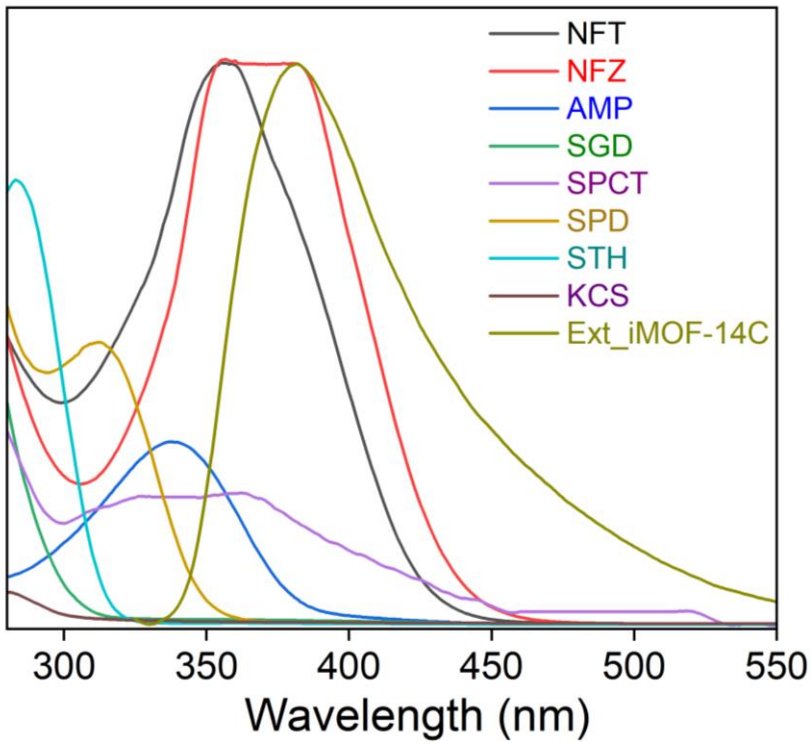

Figure S36: UV-vis absorption spectra of all antibiotics, and emission spectra of **iMOF-14C**.

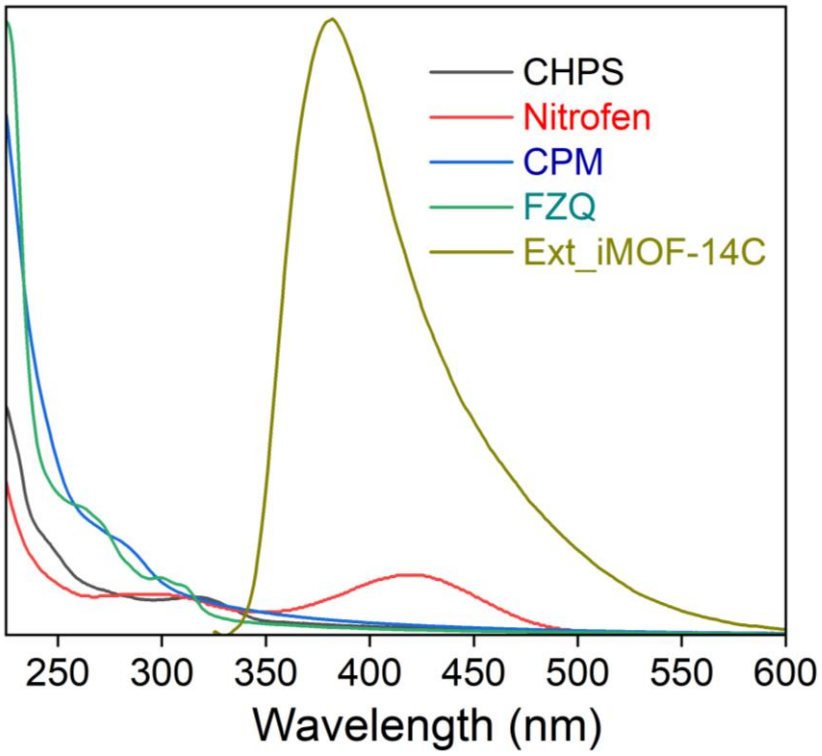

Figure S37: UV-vis absorption spectra of all pesticides, and emission spectra of **iMOF-14C**.

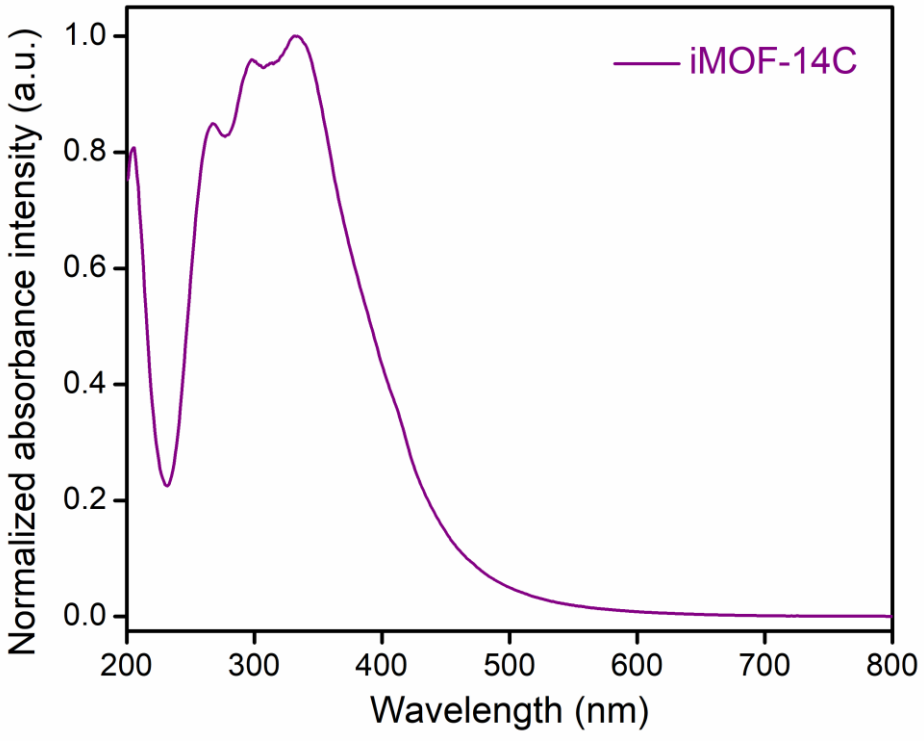

Figure S38: Solid state UV-Vis absorption spectra of **iMOF-14C**.

a)

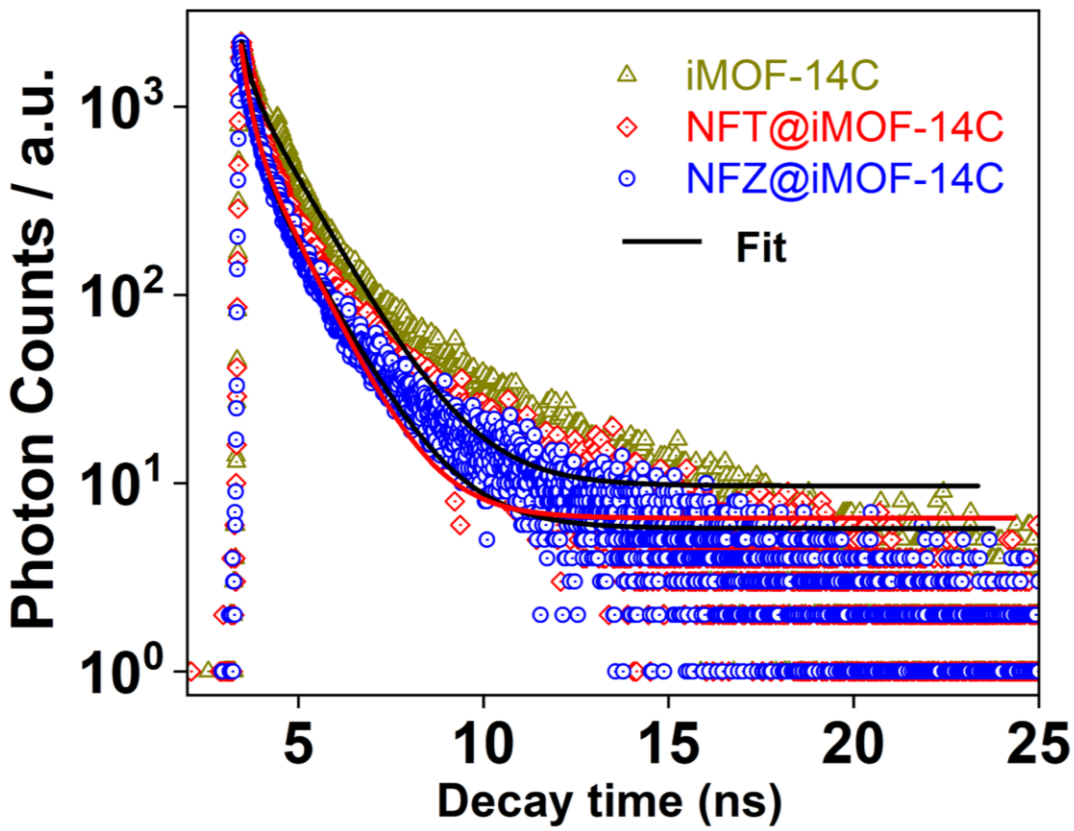

b)

Sample	t_1 (ns)	t_2 (ns)	%α_1	%α_2	R^2	t_{av} (ns)
iMOF-14C	1.26	0.24	0.0011	100.00	0.99	0.24
NFT@iMOF-14C	1.06	0.21	0.0002	99.99	0.99	0.21
NFZ@iMOF-14C	1.06	0.21	0.0001	99.99	0.99	0.21

If t_1 and t_2 are photoluminescence lifetimes for bi-exponential decay with weightage α_1 and α_2 respectively, then photoluminescence decay can be fitter using:

$$I(t) = \sum_i \alpha_i e^{(t/t_i)} \; ; i = 1, 2.$$

And the average PL would be lifetime, $t_{av} = \frac{\alpha_1 t_1^2 + \alpha_2 t_2^2}{\alpha_1 t_1 + \alpha_2 t_2}$.

Excitation Wavelength: 300 nm; Detection wavelength: 375 nm; τ (Average lifetime) = 0.21 ns [NFT@iMOF-14C]; χ^2 = 0.99 and τ = 0.28 ns [NFZ@iMOF-14C]; χ^2 = 0.99;
analyte concentration: 1 mM.

Figure S39: a) Linear fitting of the lifetime decay profiles of **iMOF-14C**; b) Details of different parameters for the lifetime measurements.

Supporting information tables:

Table S1: Comparison across literature-reported porous solids featuring NFZ sensing.

Compound	K_{sv} (M^{-1})	LOD	Reference
iMOF-14C	**9.92×10^4**	**20 ppb**	***This Work***
PCF-2	2.75×10^4	0.045 mM	*ACS Appl. Polym. Mater*. **2022**, 11, 8633–8644
BUT-12	1.1×10^5	58 ppb	*J. Am. Chem. Soc.* **2016**, *138*, 6204−6216
BUT-13	7.5×10^4	90 ppb	*J. Am. Chem. Soc.* **2016**, *138*, 6204−6216
Mg-LMOF	9.0×10^4	108 ppb	*Inorg. Chem.* **2018**, *57*, 13330−13340
Cd-TTPBA-4	4.8×10^4	N.M.	*Inorg. Chem. Commun.* **2018**, *96*, 202–205
RhB@Tb-dcpcpt	5.98×10^4	99 ppb	*ACS Appl. Mater. Interfaces* **2019**, *11*, 21201−21210
CP 1	4.4×10^4	42 ppb	*CrystEngComm*, **2019**, *21*, 6130-6135
CP 2	2.1×10^5	71 ppb	*CrystEngComm*, **2019**, *21*, 6130-6135
[Zn(L)(BDC)]	1.7×10^4	0.91 μM	*Cryst. Growth Des*., **2018**, *18*, 7173–7182.
[Cd(L)(BDC)]	4.5×10^4	0.85 μM	*Cryst. Growth Des.*, **2018**, *18*, 7173–7182.
[Cd(L)(NDC)]	1.0×10^5	75 ppb	*J. Mater. Chem. A*, **2017**, *5*, 15797–15807.
[Cd(L)(BPDC)]	1.3×10^5	60 ppb	*J. Mater. Chem. A*, **2017**, *5*, 15797–15807.
[Zn(TRZ)(DBT)]	5.2×10^4	N.M.	*Cryst. Growth Des.*, **2019**, *19*, 694–703.
[Cd(CBCD)]	9.7×10^4	85 ppb	*Dalton Trans.*, **2019**, *48*, 2683–2691.
[Zn(BCTPE)]	N/A	0.1 ppm	*J. Mater. Chem. C*, **2018**, *6*, 2983–2988.
{[Zn_2(TRZ)$_2$(DBTDC-O_2)]·DMAc}n	5.2×10^4	4.04×10^{-7} mol/L	*Cryst. Growth Des.* **2019**, *19*, 694−703
CSMCRI-2	1.30×10^5	0.7 μM	*J. Mater. Chem. A*, **2019**, *7*, 19471–19484
TMPyPE@bio-MOF-1	4.48×10^4	0.110 ppm	*J. Mater. Chem. C*, **2019**, *7*, 8383—8388
IITG-5a	1.42×10^5	156.7 nM	*Inorg. Chem. Front.*, **2022**, *9*, 859–869

N.M.: Not mentioned.

Table S2: Comparison across literature-reported porous solids featuring NFT sensing.

Compound	K_{sv} (M^{-1})	LOD	Reference
iMOF-14C	**4.5×10^4**	**100 ppb**	***This Work***
PCF-2	1.6×10^4	0.046 mM	*ACS Appl. Polym. Mater*. **2022**, 11, 8633–8644
BUT-12	3.8×10^4	N.M.	*J. Am. Chem. Soc.* **2016**, *138*, 6204−6216
BUT-13	6.0×10^4	N.M.	*J. Am. Chem. Soc.* **2016**, *138*, 6204−6216
Mg-LMOF	8.82×10^4	126 ppb	*Inorg. Chem.* **2018**, *57*, 13330−13340
Cd-TTPBA-4	6.1×10^4	N.M.	*Inorg. Chem. Commun*. **2018**, *96*, 202–205
RhB@Tb-dcpcpt	6.69×10^4	106 ppb	*ACS Appl. Mater. Interfaces* **2019**, *11*, 21201−21210
CP 1	3.4×10^4	14 ppb	*CrystEngComm*, **2019**, *21*, 6130-6135
CP 2	2.6×10^5	17 ppb	*CrystEngComm*, **2019**, *21*, 6130-6135
{[Zn_2(TRZ)$_2$(DBTDC-O_2)]·DMAc}n	1.8×10^5	3.53×10^{-7} mol/L	*Cryst. Growth Des.* **2019**, *19*, 694−703
TMPyPE@bio-MOF-1	4.42×10^4	0.134 ppm	*J. Mater. Chem. C*, **2019**, *7*, 8383—8388
IITG-5a	4.30×10^5	96.3 nM	*Inorg. Chem. Front.*, **2022**, *9*, 859–869

N.M.: Not measured.

Table S3. Crystal data and structure refinement details tabulated for **iMOF-14C.**

Crystal data

Chemical formula	$(C_{66}H_{48}N_{12}Cd)\cdot(ClO_4)\cdot(C_3H_7NO)\cdot[ClO_4\cdot 8(C_3H_7NO)$ *i.e.*, $C_{93}H_{111}CdC_{l2}N_{21}O_{17}$
M_r	1978.32
Crystal system, space group	Triclinic, *P*1
Temperature (K)	150
a, *b*, *c* (Å)	12.435 (4), 12.788 (5), 14.237 (5)
α, β, γ (°)	88.880 (9), 89.395 (9), 81.789 (9)
V (Å^3)	2240.3 (14)
Z	1
Radiation type	Mo *K*α
μ (mm^{-1})	0.39
Crystal size (mm)	0.12 × 0.10 × 0.10
Data collection	
Diffractometer	Bruker Apex3 CMOS Diffractometer
Absorption correction	Multi-scan *SADABS* (Bruker, 2016)
T_{min}, T_{max}	0.89, 0.92
No. of measured, independent and observed [$I > 2\sigma(I)$] reflections	54719, 15797, 8663
R_{int}	0.161
$(\sin\theta/\lambda)_{max}$ (Å^{-1})	0.603

Refinement

$R[F^2 > 2\sigma(F^2)]$, $wR(F^2)$, *S*	0.084, 0.244, 0.98
No. of reflections	15797
No. of parameters	959
No. of restraints	4206
H-atom treatment	H-atom parameters constrained
$\Delta\rangle_{max}$, $\Delta\rangle_{min}$ (e Å^{-3})	1.53, -0.88
Absolute structure	Refined as an inversion twin.
Absolute structure parameter	0.53 (6)

Computer programs: *APEX3* (Bruker, 2016), *APEX3*/*SAINT* (Bruker, 2016), *SAINT*/*XPREP* (Bruker, 2016), *SHELXT2018*/2 (Sheldrick, 2018), *SHELXL2018*/3 (Sheldrick, 2018), *ORTEP-3* (Farrugia, 1997) and *Mercury* (Bruno *et al.*, 2002).

References:

1. SAINT Plus; Bruker AXS Inc.: Madison, WI, 2004.

2. L. Krause, R. Herbst-Irmer, G. M. Sheldrick, D. Stalke, *J. Appl. Crystallogr*., 2015, **48**, 3−10.

3. G. M. Sheldrick, SHELXTL, Reference Manual, version 5.1; Bruker AXS Inc.: Madison, WI, 1997.

4. G. M. Sheldrick, *Acta Crystallogr., Sect. A: Found. Crystallogr*., 2008, **64**, 112−122.

5. G. M. Sheldrick, *Acta Crystallogr., Sect. C: Struct. Chem*., 2015, **71**, 3−8.

6. L. Farrugia, WinGX; University of Glasgow: Glasgow, Scotland, 2009.

7. A. L. Spek, *Acta Crystallogr. Sect. C: Struct. Chem.*, 2015, **71**, 9−18.

8. M. S. Denny, S. M. Cohen, *Angew. Chem. Int. Ed*., 2015, **54**, 9029 –9032.